BBA - Proteins and Proteomics 1869 (2021) 140583

Contents lists available at ScienceDirect

BBA - Proteins and Proteomics

journal homepage: www.elsevier.com/locate/bbapap

Molecular and cellular dynamics of the 26S proteasome

Eri Sakata [a,b,*], Markus R. Eisele [a,c], Wolfgang Baumeister [a,*]

[a] Department of Molecular Structural Biology, Max Planck Institute of Biochemistry, 82152 Martinsried, Germany
[b] Institute for Auditory Neuroscience, University Medical Center Göttingen, 37077 Göttingen, Germany
[c] Department of Biochemistry, Gene Center, Ludwig Maximilian University of Munich, 81377 Munich, Germany

ARTICLE INFO

Keywords:
26S proteasome
cryo-electron microscopy
cryo-electron tomography
structural dynamics
AAA+ ATPases
single particle analysis

ABSTRACT

In eukaryotic cells, the ubiquitin-proteasome system serves to remove proteins that are either dysfunctional or no longer needed. The 26S proteasome is a 2.5 MDa multisubunit complex comprising the 20S core particle, where degradation is executed, and one or two regulatory particles which prepare substrates for degradation. Whereas the 20S core particles of several species had been studied extensively by X-ray crystallography, the 26S holocomplex structure had remained elusive for a long time. Recent advances in single-particle cryo-electron microscopy have changed the situation and provided atomic resolution models of this intriguing molecular machine and its dynamics. Besides, cryo-electron tomography enables structural studies *in situ*, providing molecular resolution images of macromolecules inside pristinely preserved cellular environments. This has greatly contributed to our understanding of proteasome dynamics in the context of cells.

1. Introduction

The ubiquitin–proteasome pathway (UPP) is a key element of proteostasis: misfolded or otherwise defective as well as short-lived regulatory proteins are removed irreversibly by degradation [1–3]. The UPP regulates many fundamental cellular processes, such as the cell cycle, DNA repair, membrane trafficking, and signal transduction and malfunctions cause a wide variety of diseases [4–6].

The 26S proteasome operates at the executive end of the UPP. It has evolved to perform the specific degradation of an extraordinarily broad spectrum of substrates [7,8]. Being essentially non-specific itself, specificity is conferred by the covalent attachment of polyubiquitin chains to substrates. Poly-ubiquitylated substrates are then recognized by the 26S complex which degrades them into short peptides in an ATP-dependent manner [9–13].

The 26S proteasome comprises two subcomplexes: the 20S core particle (CP) and 19S regulatory particles (RPs) (Fig. 1A). The CP is formed by four stacked rings, two β-rings and two α-rings, arranged in the order αββα [14,15] (Fig. 1B). The outer α-ring is formed by seven homologous non-catalytic subunits. The inner β-ring is formed by seven homologous subunits, only three of which (β1, β2, and β5) carry the proteolytic sites in eukaryotes (Fig. 1C), whereas all seven β subunits are proteolytically active in prokaryotes. The active sites of the β subunits are located inside the catalytic chamber formed by two apposed β-rings and sequestered from the cellular environment. Access to this chamber is controlled by gates formed by the N-terminal segments of the α subunits which close off the barrel (Fig. 1D) [16–20].

In eukaryotes, several ATP-independent activators exist, such as hsPA28, hsPA200/yBlm10; however, the main regulator is the 19S RP which caps one or both ends of the 20S barrel [21]. 19S RP comprises 19 different subunits: six Regulatory-Particle AAA+ ATPases (RPT) subunits (Rpt1–6), and thirteen Regulatory Particle Non-ATPases (RPN) subunits (Rpn1-3, Rpn5–Rpn13 and Rpn15/Sem1) [22]. The Rpt subunits form structurally the core of the RPs and drive the conformational changes of the RPs during the functional cycle [23,24]. The Rpn subunits serve functions both in the recognition of poly-ubiquitylated substrates and in their deubiquitylation (DUB) before unfolding and translocation into the CP. They also coordinate the movements needed for the precise positioning of the RPs to the CP for substrate processing [24]. The 19S RP can dissociate into a base subcomplex with the AAA+ ATPases, Rpn1, Rpn2, and Rpn13, and often Rpn10, and a lid subcomplex containing the remaining non-ATPase subunits [25]. The 26S proteasome also binds several proteasome interacting proteins (PIPs) that interact transiently with the 26S proteasome, including DUBs, ubiquitin receptors, ubiquitin ligases, as well as chaperones required for assembly [22,26–33].

The structure of the CP has been studied extensively by X-ray crystallography [14,15,34,35]. However, structural studies of the holocomplex lagged behind because of its sheer complexity, its labile

* Corresponding authors at: Department of Molecular Structural Biology, Max Planck Institute of Biochemistry, 82152 Martinsried, Germany.
E-mail addresses: eri.sakata@med.uni-goettingen.de (E. Sakata), baumeist@biochem.mpg.de (W. Baumeister).

https://doi.org/10.1016/j.bbapap.2020.140583
Received 24 September 2020; Received in revised form 7 December 2020; Accepted 9 December 2020
Available online 13 December 2020

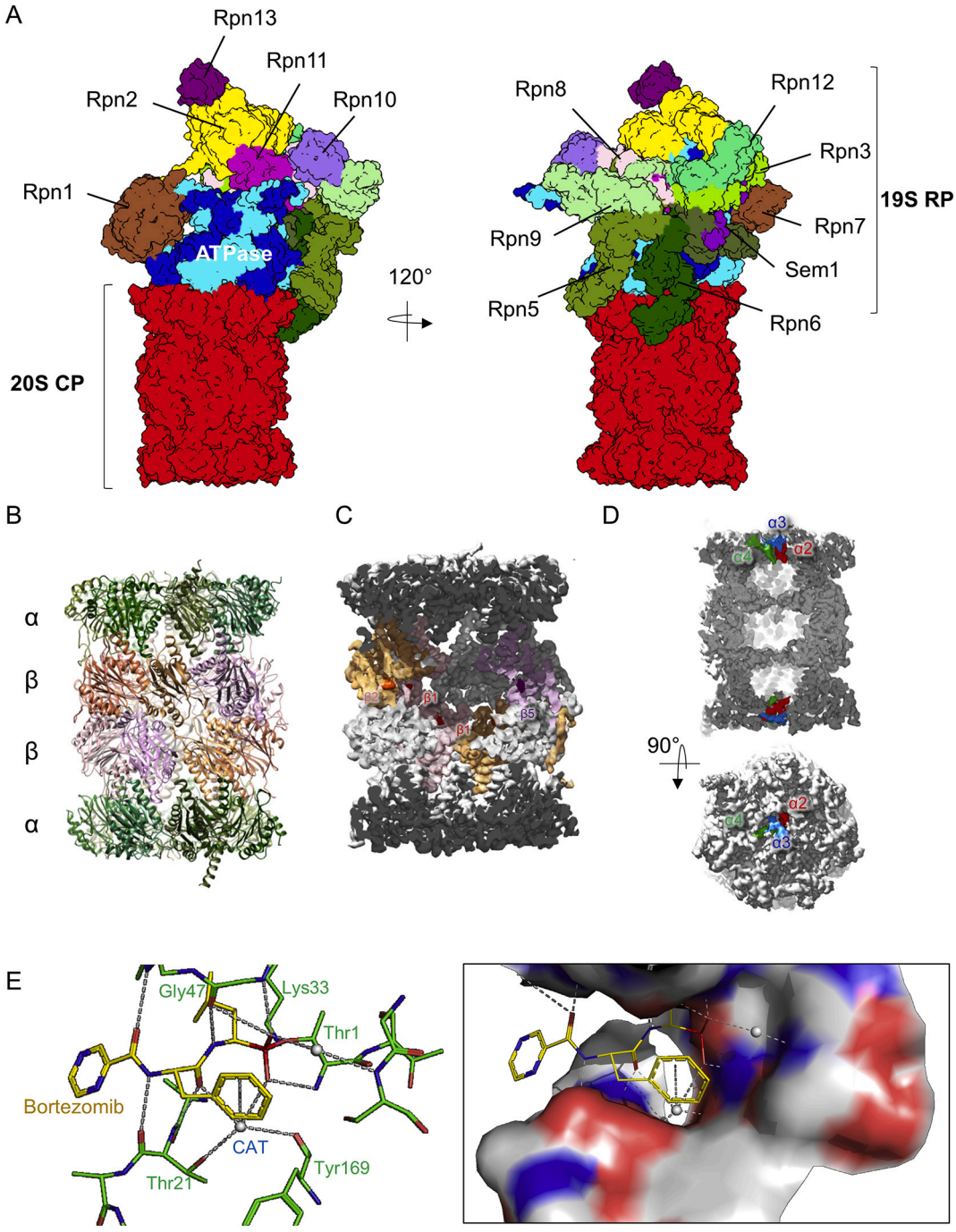

Fig. 1. (A) Molecular architecture of the yeast 26S proteasome in s1 state (EMDB ID: 3534, PDB ID:6FVT) [50]. The cryo-EM density maps are color-coded as follows: 20S CP (red), Rpt1, Rpt6, Rpt4 (blue), Rpt2, Rpt3, Rpt5 (cyan), Rpn1 (brown), Rpn2 (yellow), Rpn11(magenta), Rpn8 (plum), Rpn10 (medium purple), Rpn13 (purple), and the lid subunits (Rpn3, Rpn5, Rpn6, Rpn7, Rpn9, Rpn12, Sem1) in shades of green. (B) Structure of the 20S core particle (PDB ID:6FVT). The CP consists of two α rings at the outside and two β rings at the inside. (C) Three proteolytic sites (β1, β2, β5) face the interior of the CP cylinder. The catalytic threonine residues of the β1, β2, and β5 are colored in red, orange, and purple, and individual catalytic subunits are in pink, sandy brown, and plum, respectively. (D) The N-terminal segments of the α2, α3, and α4 are involved in gating of the CP. The N-termini of the α2, α3, and α4 are shown in red, blue, and green, respectively [16–20]. (E) Details of the chymotrypsin-like proteolytic sites (β5) and its surface charge distribution of the β5 subunit in complex with inhibitor Bortezomib (PDB ID:5LF3) in the crystal structure [81].

nature, and its dynamics [36,37]. In the past decade, structure determination by cryo-electron microscopy (EM) has become a viable alternative owing to the less demanding requirements regarding sample homogeneity. Consequently, almost all advances in our understanding of the structure of the 26S holocomplex are derived from cryo-EM single particle analysis [36,38–42] often using integrative or hybrid approaches [43–45] (Fig. 1A). Recent advances in EM technology and software for image processing and analysis [46–48] allowed to obtain structures of the human and yeast 26S proteasome at near-atomic resolutions, leading to a deeper understanding of proteasome functions [49–54].

Cellular structural biology by cryo-electron tomography (cryo-ET) has been developed to image cellular components *in situ*, i.e. in unperturbed cellular environments [55–57]. A robust workflow has been

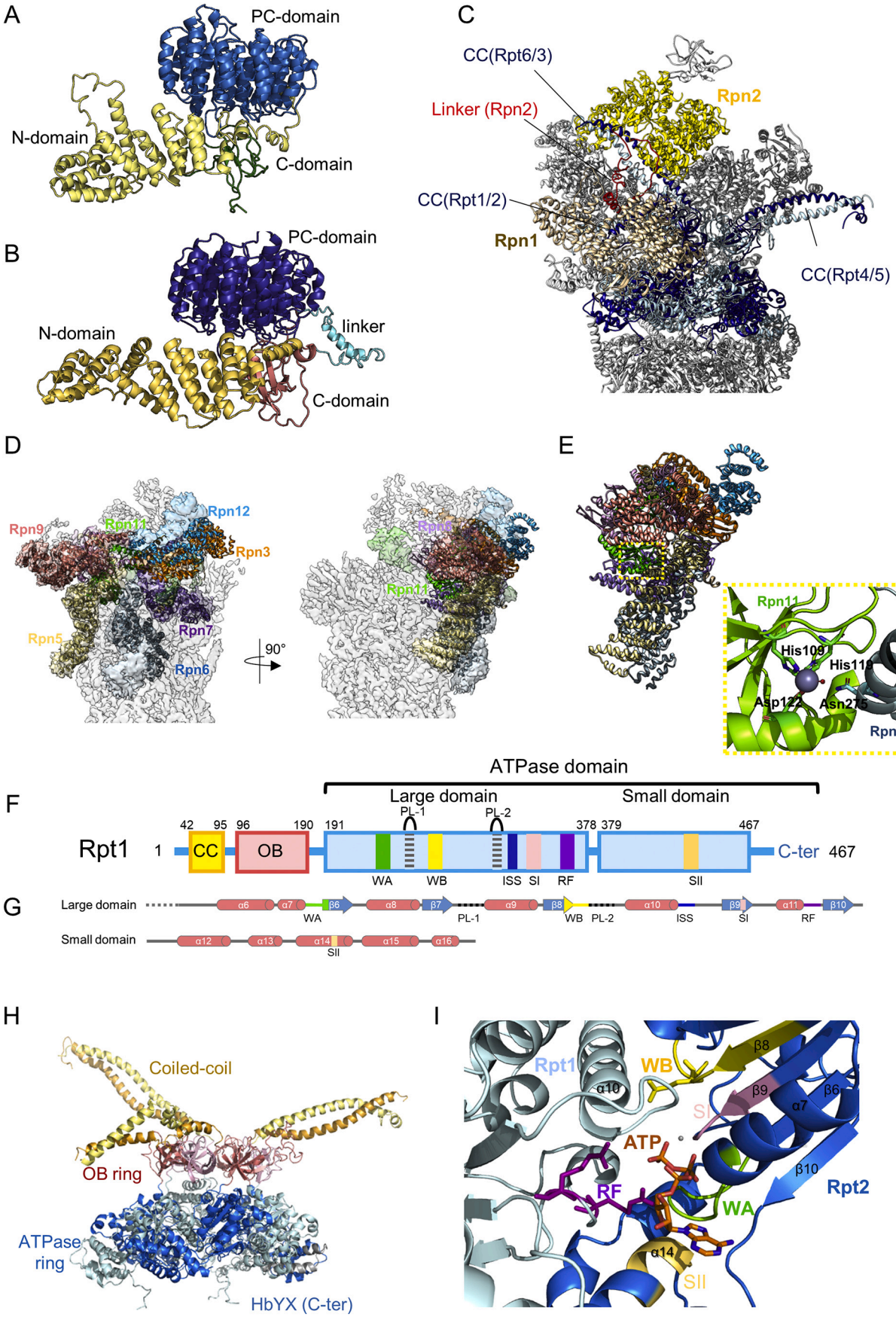

(caption on next page)

Fig. 2. Structural comparison between Rpn1 (A) and Rpn2 (B) (PDB ID:6FVT) [50,88]. Both subunits are composed of the N-terminal domain, Proteasome/Cyclosome repeats domain and the C-terminal domain. Rpn2 contains a linker between the PC- and the C-terminal domains (cyan). (C) Localization of Rpn1 (tan) and Rpn2 (yellow) in the 26S complex. The Rpn2 linker (red) extends towards Rpn1. The coiled-coil of Rpt1/2 and Rpt6/3 interacts with Rpn1 and Rpn2, respectively. (D) Structural differences of the isolated lid (PDB ID:3JCK) and the lid in the 26S proteasome holocomplex (EMDB: 3534, PDB ID: 6FVT) [42]. The lid complex alters the conformation by integrating it into the holocomplex. The isolated lid complex is shown in the ribbon model, whereas the lid complex in the 26S proteasome is shown by the surface model. The lid subunits are colored in Rpn9 (coral), Rpn5 (khaki), Rpn6 (light blue), Rpn7 (purple), Rpn3 (orange), Rpn12 (sky blue), Rpn11 (green), Rpn8 (plum), and Sem1 (forest green). (E) The active site of Rpn11 is blocked by Rpn5 in the isolated lid complex, leading to the DUB inactivation during the assembly process (PDB ID: 3JCK) [42]. (F) Domain organization of the Rpt1 subunits of the yeast 26S proteasome. Conserved structural elements are highlighted as follows: Walker A (WA), green; Walker B (WB), yellow; sensor I (SI), pink; sensor II (SII), beige; arginine finger (AF), purple; intersubunit signaling (ISS), blue; pore loop 1 (PL-1) and pore loop 2 (PL-2), black/white stripe [103,104]. (G) Secondary structures of the large (top) and small (bottom) domains. The characteristic elements are shown using the same color-code in (H). (H) Hexameric arrangement of the AAA+ ATPases of the yeast 26S proteasome [50]. The ATPase ring assembles from three dimers, Rpt1-Rpt2, Rpt6-Rpt3, and Rpt4-Rpt5. The coiled-coil domain, OB ring domain, and ATPase domain are colored in yellow/orange, pink/red, and light blue/blue, respectively. (H) The nucleotide pocket between Rpt1 and Rpt2. The nucleotide binding pocket is located at the interface of two Rpt subunits. Conserved structural elements are shown in the same color code in (H).

established allowing to target specific cellular volumes, to cut electron-transparent windows by cryo-focussed ion beam (cryo-FIB) milling [58,59], and to improve in-focus contrast using the phase plate [60,61]. Furthermore, image processing tools for extracting a maximum of information from the tomograms such as template matching [62,63] and subtomogram averaging have been developed to obtain *in situ* structures of macromolecules [64,65]. We have reported an *in situ* study of 26S proteasomes in hippocampal neurons [66], which demonstrated that it is possible to localize individual complexes with a precision of 1 – 2 nm, to assess their state of assembly and, by correlation with the aforementioned *ex situ* studies, to infer from the conformation their activity status.

In this review, we discuss the recent advances in our understanding of the conformational changes of the 26S proteasome undergoes in its functional cycle and the dynamics of its interactions within the cellular environment.

2. Proteasome assembly and structure

2.1. Structural study of the CP

The 20S CP is a C2-symmetrical cylinder-shaped multisubunit complex (Fig. 1B). The β catalytic subunits are classified as members of a family of N-terminal nucleophilic (Ntn) threonine proteases [15,67]. Archaeal and eubacterial β subunits cleave peptides after hydrophobic residues whereas eukaryotic proteasomes exhibit three distinct peptidase activities; β1 (caspase-like activity), β2 (trypsin-like activity), and β5 (chymotrypsin-like activity) (Fig. 1C) [68,69]. In lymphoid cells, catalytic subunits are replaced by their interferon-γ-inducible homologous subunits, β1i, β2i, and β5i, forming a so-called immunoproteasome [70,71]. Immunoproteasomes generate antigenic peptides with high affinity for major histocompatibility complex (MHC) class I receptors; this eventually triggers the cellular immune response [72]. Cortical thymic epithelial cells express a thymic-specific catalytic subunit β5t and form the thymoproteasome together with β1i, and β2i subunits; this variant generates peptides optimized for the positive selection of T cells [73,74].

The proteasome inhibitors that react with the active-site threonine residues of the catalytic β subunits have been developed for biochemical and cellular studies and later for clinical applications. Among those, classes of the peptide boronate (e.g., Bortezomib) and peptide epoxyketone (e.g., Carfilzomib) have been clinically applied for the treatment of multiple myeloma, mantle cell lymphoma, and solid tumors [75,76] because they suppress cell proliferation and induce the apoptosis of tumor cells by inhibiting the multiple signalling pathways [77,78]. However, acquired resistance to the proteasome inhibitors is limiting clinical applications [79,80]. Crystal structures of the CP in complex with proteasome inhibitors have greatly contributed to our understanding of how those compounds form irreversible covalent bonds with the catalytic threonine residues to inhibit catalytic reactions (Fig. 1E) [81–83]. Single point mutations of the β5 subunits found in the bortezomib-resistant cell lines induce conformational changes to the inhibitor-binding site, impairing both inhibitor-binding and catalytic activity [82]. Developments of new inhibitors or inhibitors of some of the other proteasomal subunits such as Rpn11 or Ubp6/Usp14 may resolve these problems [84].

2.2. Structure of the RP base complex

In the base complex of the RP, the six Rpt subunits assemble into a heterohexameric ATPase ring (Figs. 1A, 2F, and 2G), which sits directly on top of the α ring of the CP. Two ubiquitin receptors, Rpn10 and Rpn13, are located at the periphery of the RP and recognize the poly-ubiquitin chains bound to target substrates, whilst the other ubiquitin receptor Rpn1 is placed near the ATPase ring (Fig. 1A) [85–87]. Rpn1 and Rpn2 which are the largest subunits of the RP are composed of a toroid built from 11 Proteasome-Cyclosome (PC)-motifs; they attach to the coiled coils of Rpt1/Rpt2 and Rpt6/Rpt3 dimers, respectively (Fig. 2A and 2B) [40,88]. Rpn2 contains a linker connecting between the PC domain and the C-terminal domain, which extends towards Rpn1 (Fig. 2B and 2C). Rpn1 recruits poly-ubiquitylated substrates, both directly and indirectly [28,29,87]. It interacts with ubiquitin through toroid 1 (T1) site. Rpn1 also plays an important role as an interaction hub for proteasome interacting proteins (PIPs) [29,87,89]. It recognizes ubiquitin-like (UBL) domains of the substrate shuttling factors such as Rad23 and Dsk2, which are associated with poly-ubiquitin chain through the T1 site [87]. It has a second UBL-binding (T2) site in the PC domain where the DUB enzyme Ubp6 binds. Rpn1 alters its position to the other subunits of the RP during the ATP hydrolysis cycle via its interaction with the Rpt1/Rpt2 coiled-coil; this may be favourable for accommodating ubiquitylated substrates or PIPs [50,90,91].

2.3. Structure of the lid subcomplex of the RP

The lid complex is composed of eight subunits, six Proteasome-Cyclosome (CSN)-eIF3 (PCI), two MPN domains subunits (Rpn 11 and Rpn8), and sem1. The six PCI subunits form a horse-shoe shaped structure which holds the Rpn11/Rpn8 heterodimer in the palm of the PCI domains (Fig. 3D). The overall structure of the lid complex resembles the elF3 and CSN [92–94]. Sem1 binds to a cleft formed by Rpn3 and Rpn7. The C-termini of the PCI and MPN subunits associate into a helical bundle that holds the lid complex together [40,41,95]. Rpn11 is a JAMM metalloprotease with a modest DUB activity, while the homologous subunit Rpn8 is a pseudo protease in which the catalytic JAMM motif is missing [96,97]. The DUB activity of Rpn11 in the holocomplex was reported to be dependent on ATP hydrolysis, although Rpn11 does not contain an ATPase domain [98,99]. Substrate binding coupled with ATP hydrolysis induces conformational changes of the ATPase motors, leading to repositioning Rpn11 above the ATPase ring [24]. Ubiquitin binding on the Rpn11 catalytic site accelerates the Rpn11 DUB activity by altering the conformation of a loop that blocks the catalytic site to the 'open' state [100]. Furthermore, a cryo-EM study showed that the DUB

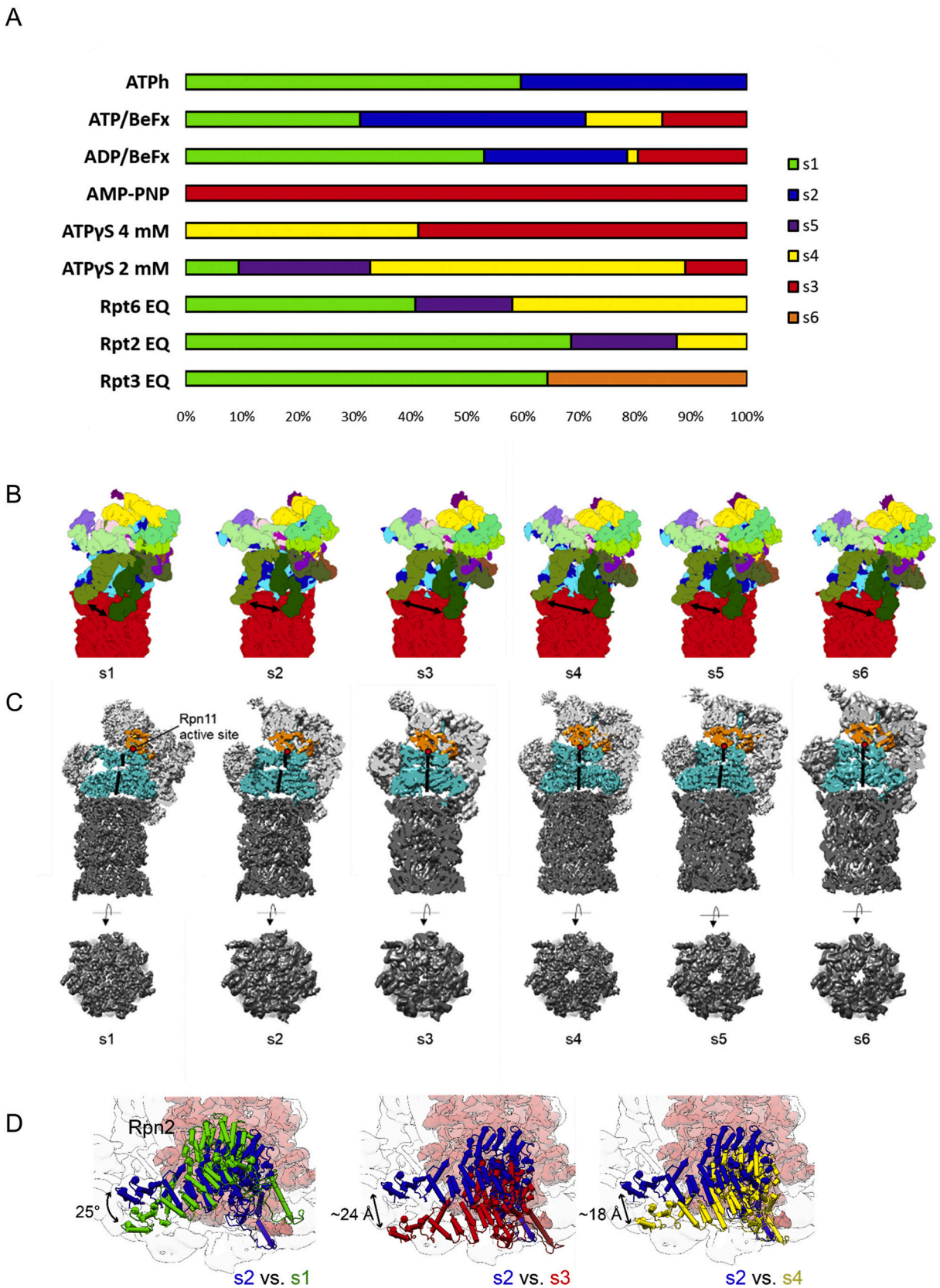

Fig. 3. (A) Summary of the abundance of proteasome RP conformations under various conditions derived from our cryo-EM data[50,122]. (B) Structural comparison of the RP conformations. Cryo-EM densities of the six published proteasome states from our studies are shown. The distance between Rpn5 (olive green) and Rpn6 (dark green) is represented as an arrow. (C) Cutaway views of the cryo-EM densities showing the position of the Rpn11 active site and the alignment of the OB ring, the AAA+ ATPase ring, and the CP in each state. The lower panel presents top views of the CP, showing the status of the gate. (D) Structural comparison of Rpn2 in different states comparing their position and orientation.

activity of Rpn11 is inhibited in the isolated lid subunit through its interaction with the lid subunit Rpn5 [42]. Rpn5 residue Asn275 forms stable tetrahedral coordination of the Zn^{2+} ion via this catalytic water molecule, restricting the catalytic site from interacting with ubiquitin chains (Fig. 2E). Rpn11 becomes activated upon incorporation into the holocomplex by disrupting the locked conformation by Rpn5 and major conformational changes in the lid assembly (Fig. 2D).

2.4. Structure of the AAA+ ATPase module of the RP

The Rpt subunits comprise an AAA+ ATPase domain at the C-terminus and an OB ring connecting to N-terminal coiled-coil motifs (Fig. 2F). Each Rpt subunit forms a dimer with its neighboring subunit (Rpt1/2, Rpt6/3, Rpt4/5) and three dimers are eventually assembled into the heterohexameric ring. The N-terminus of each Rpt subunit forms a coiled-coil within the dimer (Fig. 2H) [101]. The coiled-coil of Rpt1/2 and Rpt6/3 interacts with Rpn1 and Rpn2, respectively. The coiled-coil of Rpt4/5 is isolated and has no interaction with other subunits. However, Rpt5 interacts with poly-ubiquitin during substrate processing [102]. Each ATPase domain is composed of a large and small ATPase domain. A nucleotide-binding pocket is formed at the interface between the large and the small domains of the counter-clockwise adjacent subunit (Fig. 2I). As with other AAA-ATPase family members, the nucleotide-binding pocket is highly conserved [103], containing a Walker A, Walker B, Arg-finger and sensor 1, and sensor 2 motifs, and two pore loops [104,105] (Fig. 2F, 2G, 2I).

ATP hydrolysis is assisted by two arginine residues from the Arg-finger motif of the neighboring Rpt subunit. The arginine finger reaches towards the Walker A motif and polarizes the γ-phosphate [106]. The highly conserved glutamate of the Walker B motif polarizes a water molecule for the attack of the γ-phosphate [107]. ATP is finally hydrolyzed and energy is generated, which drives movements of the ATPase subunits. For substrate translocation, conserved aromatic-hydrophobic (Ar-Φ) pore loops play important roles in substrate unfolding and translocation [108]. The proteasome ATPases possess two sets of loops, pore-1 and pore-2, facing the central channel formed by the six ATPase subunits and interact with the incoming substrate [24,45]. As a result of the conformational change induced by ATP hydrolysis, the pore loops apply mechanical force to the substrate and pull it towards the CP [109,110]. The coordination of the entire ATPase cycle is further discussed below.

2.5. Regulatory particles of prokaryotic proteasomes

Prokaryotes operate with simpler regulatory particles. The ATPase activators are made solely of AAA+ ATPases and associate transiently with 20S proteasomes [111]. In archaea, the proteasome activating nucleotidase (PAN), and the Cdc48 homolog VCP-like ATPase (VAT) have been reported to serve as unfoldases [112–114]. PAN is the best-characterized prokaryotic proteasome activator and shares a ~40% sequence similarity with the ATPase subunits of the eukaryotic RPs. PAN forms a homohexameric ring and associates with the homo heptameric α-ring of the 20S CP. Other known prokaryotic ATP-dependent activators, M. tuberculosis mycobacterial proteasome ATPase (Mpa) [115] and its orthologue, R. erythropolis AAA+ ATPase forming ring-shaped complexes (ARC) [116], are structurally and functionally similar to PAN.

3. Structural dynamics of the 26S proteasome

3.1. High resolution structure of the 26S proteasome

Recent technological and methodological advances in cryo-EM have allowed determining high-resolution structures of the human and yeast 26S proteasome [42,49–51,54,117–120]. The recently solved cryo-EM structures of the 26S proteasome bound to either protein substrates or poly-ubiquitin chains contributed to a deeper understanding of the ATP hydrolysis mechanism and its coupling with substrate translocation [52–54,121]. Due to the pronounced dynamics, the local resolution ranges typically from ≥ 3.0 Å (e.g. 20S CP) to ≤ 6.0 Å (e.g. Rpn1, Rpn13). However, the EM densities of the CP and AAA+ ATPases are usually well resolved and showed clear densities of side chains, allowing for an unambiguous assignment and the building of atomic models [50–53,120,122]. Nucleotides could be visualized clearly as well as the surrounding residues. The structural models depict details of the nucleotide-binding pockets and the position of the central pore loops as well as the interface between CP and the AAA+ ATPases. This has contributed greatly to a mechanistic understanding of 26S proteasome function.

3.2. The conformational landscape of the 26S proteasome

Our initial cryo-EM studies in the presence of the ATP nucleotide analog, ATPγS revealed two major conformations (s1, s3) [123]. Deep classification of a very large dataset led us to find an additional conformational state (s2) [23]. Besides, additional activated conformations (s4, s5) were identified by the provision of different nucleotide analogs, such as ATPγS, AMP-PNP, and ATP/ADP-BeFx (Fig. 3A) [50,122]. Another conformation (s6) was found by mutagenesis of the Walker B motif of the Rpt3 subunit (Fig. 3A) [122]. Cryo-EM studies from several groups have reported similar conformations in yeast and human proteasome samples under different conditions [24,51–54,118–120], and these have been covered in previous reviews [124–126].

In all structures solved so far, the ATPase domains adopt an asymmetric spiral staircase arrangement where the subunits are positioned at different heights to form a helical assembly. Rpt3, in s1, s2, and s5, is positioned at the top of the staircase, whereas Rpt3 is located at the bottom position of the staircase in s4. The provision of both different nucleotide analogs and protein substrate reduce the s1 state and alter conformational distribution, indicating that an individual ATP-binding event of the Rpt subunits determines the staircase arrangement [52,53,118,122]. Thus, the 26S proteasome exists in a conformational equilibrium, and both, ATP hydrolysis and substrate engagement shift the equilibrium from the s1 ground state to the other states. Interestingly, these conformational changes are conserved not only across species belonging to different kingdoms of life but also the entire AAA+ superfamily [105,127–133]. In the cryo-EM structure of the archaeal PAN-CP complex, the hexameric PAN ATPase ring adopts a spiral staircase arrangement, as observed also in the 26S proteasome [134].

The main structural differences within these conformational states are the co-axial alignment of the ATPase rings to the CP ring and the positioning of the DUB module (Rpn 8/11). In the presence of ATP, the majority of the proteasomes stay in an inactive s1 state where the channels of the ATPase ring and CP ring are not aligned, and the DUB subunit Rpn11 is located ~25 Å away from the mouth of the ATPase channel making substrate translocation into the CP impossible (Fig. 3B and 3C) [23,38,40,45,123]. In the s2 and s5 states, the position of the ATPase ring is slightly shifted, leading to a better alignment of the axial channels. Besides, the N-terminal domains of Rpn5 and Rpn6 shifted to alter the interaction between the RP and CP. In contrast, the s3, s4, and s6 states appear configured for substrate processing due to large-scale conformational reorganizations that align Rpn11 and the ATPase pore with the axial channel of the CP [50,122]. Thus, according to their putative roles, these were referred to as a ground state (s1), a commitment (s2, s5), and a substrate processing (activated) state (s3, s4, and s6) (Fig. 3B, 3C).

Nucleotide binding pockets of those high-resolution structures have been characterized in terms of the pocket distance, which is an indicator for the openness of the intersubunit contact areas and the engagement of highly-conserved phenylalanine at the end of the H10 helix. This was previously identified as a InterSubunit Signalling (ISS) motif playing an

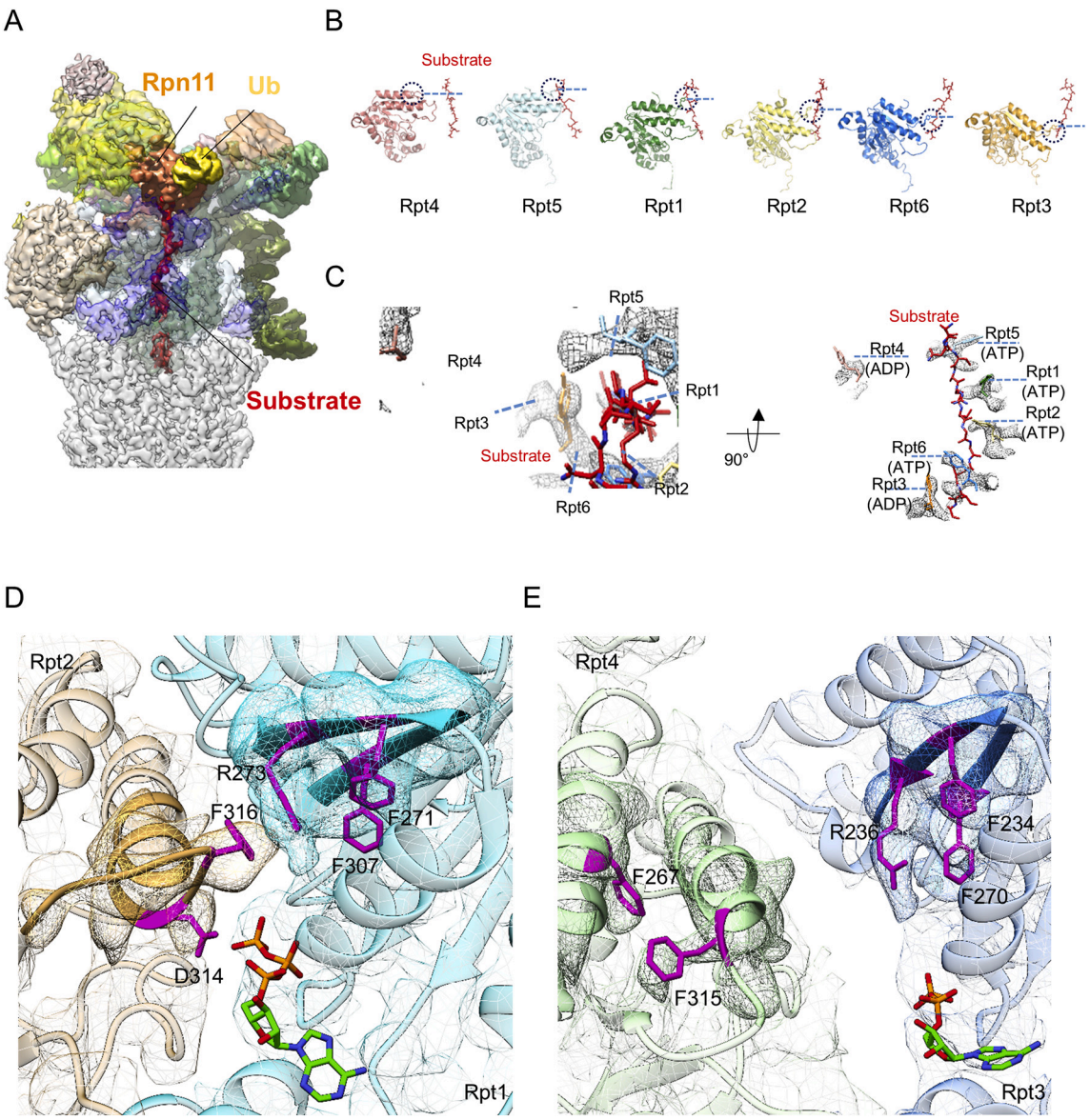

Fig. 4. (A) Structures of the ubiquitylated (yellow) substrate (red) -bound 26S proteasome showing the substrate en route to the CP (PDB ID:6EF3) [52]. To highlight the substrate, proteasomal subunits except Rpn11 are shown transparently. (B) Side views of the Rpt subunits associated with a substrate are shown in ribbon model (PDB ID:6EF3). Rpt subunits are rotated in 60° steps around the CP axis. The conserved Tyrosine residues in the pore-1 loop are highlighted by a circle and the heights of the Tyr residue are indicated by a dashed line. (C) Arrangements and interactions between the pore-1 loops and the substrate. Tyr residues are radially arranged around the substrate. The Rpt4 pore loop that bound ADP shows no interaction with the substrate, whereas the ATP bound subunits (Rpt1,2,5,6) tightly interact with the substrate. Comparison of the nucleotide binding pockets in the 'engaged' pocket (D) and 'open' pocket (E) [122]. Conserved phenylalanine residues at the H10 helix alter conformations upon nucleotide binding status. The EM density of the ATPase subunits is shown as a mesh, and side chains of the conserved Phe cluster are highlighted. Figure reproduced from [122].

important role in intersubunit communication during ATP hydrolysis [133,135] (Fig. 4D). Three distinct configurations of the nucleotide-binding pocket can be distinguished which are assigned as ATP-bound, ADP-bound, and an empty (apo) configuration. The ADP-bound subunits are typically located at the bottom of the staircase, whereas ATP-bound subunits are sequentially connected in a spiral fashion of the staircase. The apo subunits are found in the 'off' position of the staircase. The s3, s4, and s6 display similar pocket configurations, where three ATP-bound pockets are followed by two ADP-bound pockets, and by one apo pocket in a clockwise fashion. This pattern is permuted one subunit counterclockwise from s3 to s6 and again from s6 to s4. In contrast, the arrangement is preserved in s1, s2, and s5 where ATP-bound pockets in Rpt1, Rpt5, Rpt4, and Rpt3 are followed by an ADP-bound Rpt6 pocket and an apo Rpt2 pocket in a clockwise position. [50,122]. The conserved arrangements of the nucleotide-binding pockets support the sequential ATP hydrolysis model where ATP hydrolysis is coordinated within the hexamer in a sequential order around the hexameric ring.

3.3. *Gate-opening mechanisms*

Among six conformational states, the CP gate of three states (s1, s2, s3) is mostly closed, preventing substrate entry. In contract, the gates of the other three states (s4, s5, s6) are widely open (Fig. 3C). The C-terminal HbYX motifs of the AAA+ ATPases are stably docked into pockets of the α-subunits and stabilize the interaction with the CP. Insertion of the Rpt6 and Rpt1 C-termini into their respective pockets repositions the H0 helices of α2–α4 from their positions in the closed-gate states

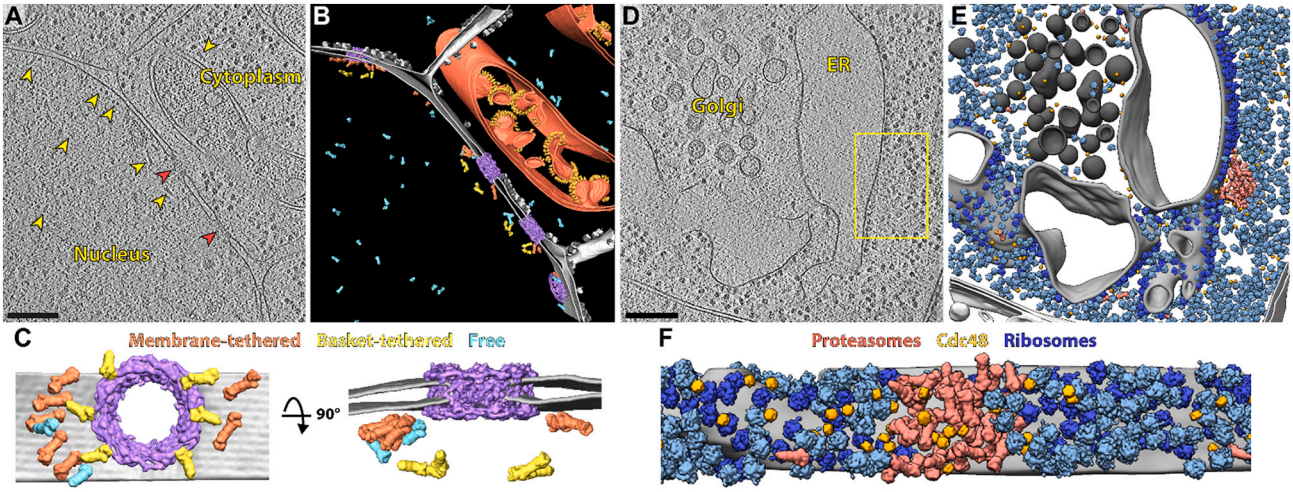

Fig. 5. Proteasome localization of the 26S proteasome in *Chlamydomonas* [145,146]. Cryo-tomographic slices (A and D) and corresponding segmentations (B and E) either at the nuclear-cytoplasm interface (A) or ER-cytoplasm interface (D). Proteasomes located in the nucleus are clustered near the inner nuclear membrane close to nuclear pore complexes (NPCs) (yellow arrows indicate proteasomes; red arrows indicate NPCs). Proteasomes in cytoplasm cluster at the ER membrane together with Cdc48. (C) Close-up tomographic views of the proteasomes in the vicinity of the NPC. The NPC is surrounded by free (blue), basket-tethered (yellow), and membrane tethered (orange) proteasomes. (F) Proteasomes and Cdc48 form micro-compartments excluding ribosomes (blue).

[51,52,122]. A mutagenesis study has shown that the deletion of the Rpt6 and Rpt1 C-termini synergistically impairs peptidase activity, leading to a growth defect *in vivo* [122]. The C-terminal tails of the AAA+ ATPases change position upon ATP binding/hydrolysis, and stimulate gate opening by disrupting the interaction network of the N-termini of the α subunits involved in gate closing/opening.

3.4. Substrate processing of the proteasome

High-resolution structures of substrate-bound proteasomes have advanced our understanding of how the Rpt subunits interact with polypeptide chains and how ATP hydrolysis is coordinated and changes conformations during substrate processing (Fig. 4A) [52,53]. Martin and colleagues determined the substrate-bound yeast 26S proteasome structures which were stalled by inhibiting the DUB activity of Rpn 11 with a Zinc chelator [52]. The proteasomes exhibit four distinct s4-like states (1D*, 5D, 5T, and 4D) with different nucleotide binding configurations. The stalled structure has an ubiquitin moiety bound to Rpn11; Interestingly, the Ins-1 loop of Rpn11 near the catalytic site is stabilized by the N-terminal helix of Rpt5 to activate Rpn11. In another cryo-EM study of a substrate-bound human 26S proteasome from Mao and his colleagues, they determined the substrate-bound structures in seven different conformational states (EA1, EA2, EB, EC1, EC2, ED1, and ED2). In addition to the ubiquitin density bound to Rpn11, further ubiquitin densities were observed; a density near the Rpt4/Rpt5 N-terminal coiled-coil and another density near Rpn1. The additional density near Rpn1 is close to the previously reported Ubp6 ubiquitin-like domain binding site (T2) rather than the ubiquitin binding site (T1), which was identified previously by NMR and mutagenesis studies [87]. Other cryo-EM studies using poly-ubiquitin chains without substrate (K48-tetraubiquitin or M1-hexaubiquitin) described that binding of poly-ubiquitin itself can induce the conformational change of the proteasome [54,121], despite elegant kinetic experiments have shown that substrate contact with the ATPase motor triggers the conformational change [136].

The ATPase ring of the substrate-bound 26S proteasome structures shares a spiral staircase conformation (Fig. 4B and 4C). The unfolded substrate travels through the central channel to the CP presenting its side chains radially toward the pore loops. The helical array of the pore loops establishes a tight grip on the substrate. The position of the pore loops is regulated by the nucleotide binding status, in which the ATP-bound subunits are firmly bound to the substrate [52,53]. The conserved Tyr residues on the pore-1 loop of each subunit intercalate with the backbone of the substrate. The geometry of the nucleotide-binding states within the hexameric ring is similar to the activated states (s3, s4 and, s6) in our studies [122]. The identical permutation pattern of the nucleotide binding pockets and arrangement of the pore-loop also suggested also that ATP hydrolysis progresses sequentially.

Thus, the existing studies support a hand-over-hand model where substrate translocation is powered by the sequential ATP hydrolysis and phosphate release such that the polypeptide chain is moved through the central channel by being handed over from one subunit to a neighbouring one [52,105,124].

3.5. In situ structural study of the 26S proteasome

Recent advances in cryo-electron tomography (cryo-ET) made it possible to study macromolecular and supramolecular assemblies *in situ* in their functional cellular environments [55,57]. Studies with hippocampal neurons, grown on EM grids, demonstrated that resolutions can be attained that allow not only determining the assembly status of individual 26S proteasomes (i.e. single capped vs. double capped) but also to infer from their conformation their activity status (i.e. ground state vs. substrate processing state) [66].

3.6. In situ studies of the 26S proteasome in Chlamydomonas

Earlier studies had shown that the unicellular green alga *Chlamydomonas reinhardtii* has some advantages facilitating cryo-ET studies: it has an almost deterministic organelle topology and its cytoplasm and nucleoplasm are less crowded than in most other eukaryotic cells [137–139]. 26S proteasomes are found in both, the cytoplasm and the nucleus. In the nucleus, they are highly enriched in the vicinity of the inner membrane of the nuclear envelope and next to nuclear pore complexes (NPC) (Fig. 5A and B). Two distinct subpopulations of NPC-associated 26S proteasomes are observed: One is tethered to the inner membrane near the periphery of the NPCs and another one tethered to the nuclear basket (Fig. 5C) [145]. The basket-bound proteasomes are likely involved in the surveillance of nuclear import and export, whereas the membrane-tethered population, which is located near the junction of the outer and inner membrane, has been implicated in controlling the different protein compositions of the two membranes.

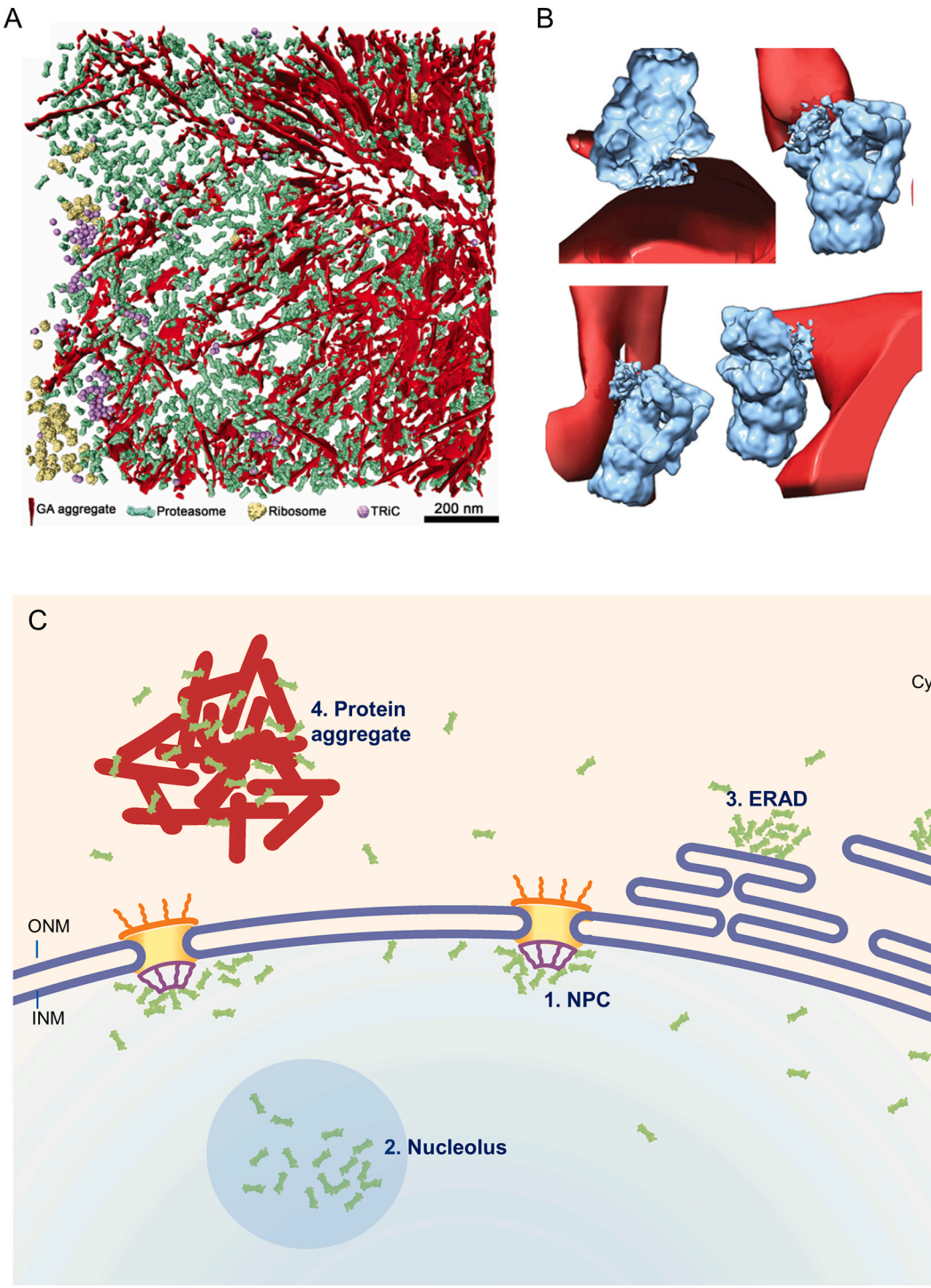

Fig. 6. 3D rendering of poly-GA aggregates within a neuron, and its relationship to various macromolecular complexes [140]. The aggregate and macromolecules are depicted in the following colors: poly-GA aggregates (red), proteasomes (green), Ribosomes (yellow), and TRiC (plum). (B) Examples of direct interactions between the aggregate material and the proteasomes. Proteasomes touching poly-GA aggregate in the tomogram are shown. (C) Schematic representation of the proteasome localization in the cells, which have been observed *in situ* cryo-TM. Proteasomes (green) cluster near the NPCs, ER membrane (Chlamydomonas), poly-GA aggregates (Neuron), and nucleolus (HCT cell under hyperosmotic stress).

Cytosolic 26S proteasomes preferably cluster on the surface of the rough endoplasmatic reticulum (ER) and colocalize with the protein segregase Cdc48, which works upstream of the proteasome in ER associated degradation (ERAD) (Fig. 5D and 5E) [146]. These degradation microcompartments which typically comprise 30-50 copies of the 26S complexes, are devoid of ER-bound ribosomes and are spatially segregated from the secretory pathway (Fig. 5F). The 26S complexes next to the ER membrane are mostly in an active conformation suggesting that they are directly involved in extracting ERAD substrates for subsequent degradation.

3.7. *Impairment of the proteasome function in neurotoxic aggregates*

Many studies have demonstrated that in several neurodegenerative

diseases such as Alzheimer's disease, Parkinson's disease, Huntington disease, amyotrophic lateral sclerosis (ALS) the UPS is impaired [6]. For example, in ALS and frontotemporal dementia, an expansion in a non-coding region of the C9orf72 gene results in the translation of toxic products. The aberrant translation product contains glycine-alanine dipeptide repeats (poly-GA). Cryo-ET analysis of poly-GA aggregates in neurons showed that they consist of twisted polymorphic ribbons (Fig. 6A) [140]. Inside the aggregate material, a massive accumulation of 26S proteasomes was observed, whereas other macromolecular complexes such as ribosomes and TRiC/CCT are excluded and located at the periphery of the aggregate. Classification of 26S particles revealed that the proteasomes directly attached to the poly-GA aggregate are mostly in the s4 conformation (Fig. 6B), indicating that the proteasomes are actively trying to degrade the poly-GA aggregate. Most likely, the proteasomes become stalled because the poly-GA repeats are resistant to unfolding and therefore cannot be translocated into the 20S core for degradation [141,142]. The massive accumulation and the stalling of the proteasomes deplete the cellular pool of degradation-competent proteasomes and thereby affect cellular protein quality control.

A recent study showed that, under acute hyperosmotic stress, proteasomes form nuclear clusters that do not co-localized with previously known nuclear bodies such as promyelocytic leukemia protein nuclear bodies and Cajal bodies [143]. Proteasome-containing foci are membrane-less organelles containing ubiquitylated proteins, p97, and several PIPs, and are involved in the clearance of ribosomal proteins.

Altogether, these *in situ* cryo-ET studies show that, to eliminate non-functional or aggregation-prone proteins, proteasomes form membrane-less proteolytic clusters allowing the cell to rapidly degrade dysfunctional proteins upon various stresses (Fig. 6C).

4. Conclusion

For quite a long time the 26S proteasome remained an enigmatic structure [144]. In recent years, advances in cryo-EM single particle analysis have allowed us to obtain high resolution structures of this dynamic molecular machine. During its functional cycle, from the initial recognition and binding of ubiquitylated substrates to their deubiquitylation, unfolding, and translocation into the degradation chamber of the core 20S complex, the regulatory particle undergoes a sequence of large scale conformational changes. *In situ* structural studies by cryo-ET are a rather new emerging field but the few studies performed so far have already demonstrated the discovery potential of this approach. A comprehensive charting of cellular landscapes will provide unprecedented insights into the molecular interaction networks underlying cellular functions.

Author statement

ES and MRE prepared figures. All authors contributed to manuscript preparation.

Declaration of Competing Interest

The authors declare that they have no known competing financial interests or personal relationships that could have appeared to influence the work reported in this paper.

Acknowledgements

The authors thank B. Engel and R. Fernández-Busnadiego for providing figures. This work was supported by the Deutsche Forschungsgemeinschaft (DFG, German Science Foundation) through Germany's Excellence Strategy - EXC 2067/1- 390729940 and CRC889/ Project A11to E.S,. and SFB-1035/Project A01 to W.B. and E.S. E.S. acknowledges financial support from Marie Curie Career Integration grant (PCIG14-GA-2013-631577).

References

[1] A. Hershko, A. Ciechanover, A. Varshavsky, Basic medical research award. The ubiquitin system, Nat. Med. 6 (2000) 1073–1081.
[2] M. Hochstrasser, Ubiquitin-dependent protein degradation, Annu. Rev. Genet. 30 (1996) 405–439.
[3] A. Hershko, A. Ciechanover, The ubiquitin system, Annu. Rev. Biochem. 67 (1998) 425–479.
[4] B. Haendler, S. Jentsch, The ubiquitin system in health and disease, in: Preface, Ernst Schering Found Symp Proc, 2008. V-VI.
[5] D. Popovic, D. Vucic, I. Dikic, Ubiquitination in disease pathogenesis and treatment, Nat. Med. 20 (2014) 1242–1253.
[6] N.P. Dantuma, L.C. Bott, The ubiquitin-proteasome system in neurodegenerative diseases: precipitating factor, yet part of the solution, Front. Mol. Neurosci. 7 (2014) 70.
[7] M.M. Savitski, N. Zinn, M. Faelth-Savitski, D. Poeckel, S. Gade, I. Becher, M. Muelbaier, A.J. Wagner, K. Strohmer, T. Werner, S. Melchert, M. Petretich, A. Rutkowska, J. Vappiani, H. Franken, M. Steidel, G.M. Sweetman, O. Gilan, E.Y. N. Lam, M.A. Dawson, R.K. Prinjha, P. Grandi, G. Bergamini, M. Bantscheff, Multiplexed proteome dynamics profiling reveals mechanisms controlling protein homeostasis, Cell 173 (2018) 260–274, e225.
[8] P. Grandi, M. Bantscheff, Advanced proteomics approaches to unravel protein homeostasis, Drug Discov. Today Technol. 31 (2019) 99–108.
[9] W. Baumeister, J. Walz, F. Zuhl, E. Seemuller, The proteasome: paradigm of a self-compartmentalizing protease, Cell 92 (1998) 367–380.
[10] D. Voges, P. Zwickl, W. Baumeister, The 26S proteasome: a molecular machine designed for controlled proteolysis, Annu. Rev. Biochem. 68 (1999) 1015–1068.
[11] A.F. Kisselev, T.N. Akopian, K.M. Woo, A.L. Goldberg, The sizes of peptides generated from protein by mammalian 26 and 20 S proteasomes. Implications for understanding the degradative mechanism and antigen presentation, J. Biol. Chem. 274 (1999) 3363–3371.
[12] K. Tanaka, The proteasome: overview of structure and functions, Proc. Jpn. Acad. Ser. B Phys. Biol. Sci. 85 (2009) 12–36.
[13] R.J. Tomko Jr., M. Hochstrasser, Molecular architecture and assembly of the eukaryotic proteasome, Annu. Rev. Biochem. 82 (2013) 415–445.
[14] J. Lowe, D. Stock, B. Jap, P. Zwickl, W. Baumeister, R. Huber, Crystal structure of the 20S proteasome from the archaeon T. acidophilum at 3.4 A resolution, Science 268 (1995) 533–539.
[15] E. Seemuller, A. Lupas, D. Stock, J. Lowe, R. Huber, W. Baumeister, Proteasome from Thermoplasma acidophilum: a threonine protease, Science 268 (1995) 579–582.
[16] M. Groll, M. Bajorek, A. Kohler, L. Moroder, D.M. Rubin, R. Huber, M. H. Glickman, D. Finley, A gated channel into the proteasome core particle, Nat. Struct. Biol. 7 (2000) 1062–1067.
[17] F.G. Whitby, E.I. Masters, L. Kramer, J.R. Knowlton, Y. Yao, C.C. Wang, C.P. Hill, Structural basis for the activation of 20S proteasomes by 11S regulators, Nature 408 (2000) 115–120.
[18] A. Forster, E.I. Masters, F.G. Whitby, H. Robinson, C.P. Hill, The 1.9 A structure of a proteasome-11S activator complex and implications for proteasome-PAN/PA700 interactions, Mol. Cell 18 (2005) 589–599.
[19] D.M. Smith, S.C. Chang, S. Park, D. Finley, Y. Cheng, A.L. Goldberg, Docking of the proteasomal ATPases' carboxyl termini in the 20S proteasome's alpha ring opens the gate for substrate entry, Mol. Cell 27 (2007) 731–744.
[20] J. Rabl, D.M. Smith, Y. Yu, S.C. Chang, A.L. Goldberg, Y. Cheng, Mechanism of gate opening in the 20S proteasome by the proteasomal ATPases, Mol. Cell 30 (2008) 360–368.
[21] B.M. Stadtmueller, C.P. Hill, Proteasome activators, Mol. Cell 41 (2011) 8–19.
[22] D. Finley, Recognition and processing of ubiquitin-protein conjugates by the proteasome, Annu. Rev. Biochem. 78 (2009) 477–513.
[23] P. Unverdorben, F. Beck, P. Sledz, A. Schweitzer, G. Pfeifer, J.M. Plitzko, W. Baumeister, F. Forster, Deep classification of a large cryo-EM dataset defines the conformational landscape of the 26S proteasome, Proc. Natl. Acad. Sci. U. S. A. 111 (2014) 5544–5549.
[24] M.E. Matyskiela, G.C. Lander, A. Martin, Conformational switching of the 26S proteasome enables substrate degradation, Nat. Struct. Mol. Biol. 20 (2013) 781–788.
[25] M.H. Glickman, D.M. Rubin, O. Coux, I. Wefes, G. Pfeifer, Z. Cjeka, W. Baumeister, V.A. Fried, D. Finley, A subcomplex of the proteasome regulatory particle required for ubiquitin-conjugate degradation and related to the COP9-signalosome and eIF3, Cell 94 (1998) 615–623.
[26] E. Sakata, F. Stengel, K. Fukunaga, M. Zhou, Y. Saeki, F. Forster, W. Baumeister, K. Tanaka, C.V. Robinson, The catalytic activity of Ubp6 enhances maturation of the proteasomal regulatory particle, Mol. Cell 42 (2011) 637–649.
[27] S. Elsasser, D. Chandler-Militello, B. Muller, J. Hanna, D. Finley, Rad23 and Rpn10 serve as alternative ubiquitin receptors for the proteasome, J. Biol. Chem. 279 (2004) 26817–26822.
[28] Y. Saeki, T. Sone, A. Toh-e, H. Yokosawa, Identification of ubiquitin-like protein-binding subunits of the 26S proteasome, Biochem. Biophys. Res. Commun. 296 (2002) 813–819.
[29] S. Elsasser, R.R. Gali, M. Schwickart, C.N. Larsen, D.S. Leggett, B. Muller, M. T. Feng, F. Tubing, G.A. Dittmar, D. Finley, Proteasome subunit Rpn1 binds ubiquitin-like protein domains, Nat. Cell Biol. 4 (2002) 725–730.
[30] H.C. Besche, W. Haas, S.P. Gygi, A.L. Goldberg, Isolation of mammalian 26S proteasomes and p97/VCP complexes using the ubiquitin-like domain from HHR23B reveals novel proteasome-associated proteins, Biochemistry 48 (2009) 2538–2549.

[31] J. Hanna, D. Finley, A proteasome for all occasions, FEBS Lett. 581 (2007) 2854–2861.
[32] D.S. Leggett, J. Hanna, A. Borodovsky, B. Crosas, M. Schmidt, R.T. Baker, T. Walz, H. Ploegh, D. Finley, Multiple associated proteins regulate proteasome structure and function, Mol. Cell 10 (2002) 495–507.
[33] R. Verma, S. Chen, R. Feldman, D. Schieltz, J. Yates, J. Dohmen, R.J. Deshaies, Proteasomal proteomics: identification of nucleotide-sensitive proteasome-interacting proteins by mass spectrometric analysis of affinity-purified proteasomes, Mol. Biol. Cell 11 (2000) 3425–3439.
[34] M. Groll, L. Ditzel, J. Lowe, D. Stock, M. Bochtler, H.D. Bartunik, R. Huber, Structure of 20S proteasome from yeast at 2.4 A resolution, Nature 386 (1997) 463–471.
[35] M. Unno, T. Mizushima, Y. Morimoto, Y. Tomisugi, K. Tanaka, N. Yasuoka, T. Tsukihara, The structure of the mammalian 20S proteasome at 2.75 A resolution, Structure 10 (2002) 609–618.
[36] J. Walz, A. Erdmann, M. Kania, D. Typke, A.J. Koster, W. Baumeister, 26S proteasome structure revealed by three-dimensional electron microscopy, J. Struct. Biol. 121 (1998) 19–29.
[37] J.M. Peters, Z. Cejka, J.R. Harris, J.A. Kleinschmidt, W. Baumeister, Structural features of the 26 S proteasome complex, J. Mol. Biol. 234 (1993) 932–937.
[38] S. Nickell, F. Beck, S.H. Scheres, A. Korinek, F. Forster, K. Lasker, O. Mihalache, N. Sun, I. Nagy, A. Sali, J.M. Plitzko, J.M. Carazo, M. Mann, W. Baumeister, Insights into the molecular architecture of the 26S proteasome, Proc. Natl. Acad. Sci. U. S. A. 106 (2009) 11943–11947.
[39] S. Bohn, F. Beck, E. Sakata, T. Walzthoeni, M. Beck, R. Aebersold, F. Forster, W. Baumeister, S. Nickell, Structure of the 26S proteasome from Schizosaccharomyces pombe at subnanometer resolution, Proc. Natl. Acad. Sci. U. S. A. 107 (2010) 20992–20997.
[40] F. Beck, P. Unverdorben, S. Bohn, A. Schweitzer, G. Pfeifer, E. Sakata, S. Nickell, J.M. Plitzko, E. Villa, W. Baumeister, F. Forster, Near-atomic resolution structural model of the yeast 26S proteasome, Proc. Natl. Acad. Sci. U. S. A. 109 (2012) 14870–14875.
[41] R.J. Tomko Jr., D.W. Taylor, Z.A. Chen, H.W. Wang, J. Rappsilber, M. Hochstrasser, A Single alpha helix drives extensive remodeling of the proteasome lid and completion of regulatory particle assembly, Cell 163 (2015) 432–444.
[42] C.M. Dambacher, E.J. Worden, M.A. Herzik, A. Martin, G.C. Lander, Atomic structure of the 26S proteasome lid reveals the mechanism of deubiquitinase inhibition, Elife 5 (2016) e13027.
[43] K. Lasker, F. Forster, S. Bohn, T. Walzthoeni, E. Villa, P. Unverdorben, F. Beck, R. Aebersold, A. Sali, W. Baumeister, Molecular architecture of the 26S proteasome holocomplex determined by an integrative approach, Proc. Natl. Acad. Sci. U. S. A. 109 (2012) 1380–1387.
[44] E. Sakata, S. Bohn, O. Mihalache, P. Kiss, F. Beck, I. Nagy, S. Nickell, K. Tanaka, Y. Saeki, F. Forster, W. Baumeister, Localization of the proteasomal ubiquitin receptors Rpn10 and Rpn13 by electron cryomicroscopy, Proc. Natl. Acad. Sci. U. S. A. 109 (2012) 1479–1484.
[45] G.C. Lander, E. Estrin, M.E. Matyskiela, C. Bashore, E. Nogales, A. Martin, Complete subunit architecture of the proteasome regulatory particle, Nature 482 (2012) 186–191.
[46] W. Kuhlbrandt, Biochemistry. The resolution revolution, Science 343 (2014) 1443–1444.
[47] X.C. Bai, G. McMullan, S.H. Scheres, How cryo-EM is revolutionizing structural biology, Trends Biochem. Sci. 40 (2015) 49–57.
[48] S.H. Scheres, RELION: implementation of a Bayesian approach to cryo-EM structure determination, J. Struct. Biol. 180 (2012) 519–530.
[49] A. Schweitzer, A. Aufderheide, T. Rudack, F. Beck, G. Pfeifer, J.M. Plitzko, E. Sakata, K. Schulten, F. Forster, W. Baumeister, Structure of the human 26S proteasome at a resolution of 3.9 A, Proc. Natl. Acad. Sci. U. S. A. 113 (2016) 7816–7821.
[50] M. Wehmer, T. Rudack, F. Beck, A. Aufderheide, G. Pfeifer, J.M. Plitzko, F. Forster, K. Schulten, W. Baumeister, E. Sakata, Structural insights into the functional cycle of the ATPase module of the 26S proteasome, Proc. Natl. Acad. Sci. U. S. A. 114 (2017) 1305–1310.
[51] S. Chen, J. Wu, Y. Lu, Y.B. Ma, B.H. Lee, Z. Yu, Q. Ouyang, D.J. Finley, M. W. Kirschner, Y. Mao, Structural basis for dynamic regulation of the human 26S proteasome, Proc. Natl. Acad. Sci. U. S. A. 113 (2016) 12991–12996.
[52] A.H. de la Pena, E.A. Goodall, S.N. Gates, G.C. Lander, A. Martin, Substrate-engaged 26S proteasome structures reveal mechanisms for ATP-hydrolysis-driven translocation, Science (2018) 362.
[53] Y. Dong, S. Zhang, Z. Wu, X. Li, W.L. Wang, Y. Zhu, S. Stoilova-McPhie, Y. Lu, D. Finley, Y. Mao, Cryo-EM structures and dynamics of substrate-engaged human 26S proteasome, Nature 565 (2019) 49–55.
[54] Z. Ding, C. Xu, I. Sahu, Y. Wang, Z. Fu, M. Huang, C.C.L. Wong, M.H. Glickman, Y. Cong, Structural snapshots of 26S proteasome reveal tetraubiquitin-induced conformations, Mol. Cell 73 (2019) 1150–1161, e1156.
[55] V. Lucic, A. Rigort, W. Baumeister, Cryo-electron tomography: the challenge of doing structural biology in situ, J. Cell Biol. 202 (2013) 407–419.
[56] S. Asano, B.D. Engel, W. Baumeister, In situ cryo-electron tomography: A post-reductionist approach to structural biology, J. Mol. Biol. 428 (2016) 332–343.
[57] M. Beck, W. Baumeister, Cryo-electron tomography: can it reveal the molecular sociology of cells in atomic detail? Trends Cell Biol. 26 (2016) 825–837.
[58] A. Rigort, F.J. Bauerlein, E. Villa, M. Eibauer, T. Laugks, W. Baumeister, J. M. Plitzko, Focused ion beam micromachining of eukaryotic cells for cryoelectron tomography, Proc. Natl. Acad. Sci. U. S. A. 109 (2012) 4449–4454.
[59] E. Villa, M. Schaffer, J.M. Plitzko, W. Baumeister, Opening windows into the cell: focused-ion-beam milling for cryo-electron tomography, Curr. Opin. Struct. Biol. 23 (2013) 771–777.
[60] R. Danev, B. Buijsse, M. Khoshouei, J.M. Plitzko, W. Baumeister, Volta potential phase plate for in-focus phase contrast transmission electron microscopy, Proc. Natl. Acad. Sci. U. S. A. 111 (2014) 15635–15640.
[61] Y. Fukuda, U. Laugks, V. Lucic, W. Baumeister, R. Danev, Electron cryotomography of vitrified cells with a Volta phase plate, J. Struct. Biol. 190 (2015) 143–154.
[62] J. Bohm, A.S. Frangakis, R. Hegerl, S. Nickell, D. Typke, W. Baumeister, Toward detecting and identifying macromolecules in a cellular context: template matching applied to electron tomograms, Proc. Natl. Acad. Sci. U. S. A. 97 (2000) 14245–14250.
[63] A.S. Frangakis, J. Bohm, F. Forster, S. Nickell, D. Nicastro, D. Typke, R. Hegerl, W. Baumeister, Identification of macromolecular complexes in cryoelectron tomograms of phantom cells, Proc. Natl. Acad. Sci. U. S. A. 99 (2002) 14153–14158.
[64] Y. Chen, S. Pfeffer, J.J. Fernandez, C.O. Sorzano, F. Forster, Autofocused 3D classification of cryoelectron subtomograms, Structure 22 (2014) 1528–1537.
[65] Y. Chen, S. Pfeffer, T. Hrabe, J.M. Schuller, F. Forster, Fast and accurate reference-free alignment of subtomograms, J. Struct. Biol. 182 (2013) 235–245.
[66] S. Asano, Y. Fukuda, F. Beck, A. Aufderheide, F. Forster, R. Danev, W. Baumeister, Proteasomes. A molecular census of 26S proteasomes in intact neurons, Science 347 (2015) 439–442.
[67] P. Chen, M. Hochstrasser, Biogenesis, structure and function of the yeast 20S proteasome, EMBO J. 14 (1995) 2620–2630.
[68] C.S. Arendt, M. Hochstrasser, Identification of the yeast 20S proteasome catalytic centers and subunit interactions required for active-site formation, Proc. Natl. Acad. Sci. U. S. A. 94 (1997) 7156–7161.
[69] W. Heinemeyer, M. Fischer, T. Krimmer, U. Stachon, D.H. Wolf, The active sites of the eukaryotic 20 S proteasome and their involvement in subunit precursor processing, J. Biol. Chem. 272 (1997) 25200–25209.
[70] M. Gaczynska, K.L. Rock, A.L. Goldberg, Gamma-interferon and expression of MHC genes regulate peptide hydrolysis by proteasomes, Nature 365 (1993) 264–267.
[71] M. Aki, N. Shimbara, M. Takashina, K. Akiyama, S. Kagawa, T. Tamura, N. Tanahashi, T. Yoshimura, K. Tanaka, A. Ichihara, Interferon-gamma induces different subunit organizations and functional diversity of proteasomes, J. Biochem. 115 (1994) 257–269.
[72] K. Tanaka, M. Kasahara, The MHC class I ligand-generating system: roles of immunoproteasomes and the interferon-gamma-inducible proteasome activator PA28, Immunol. Rev. 163 (1998) 161–176.
[73] S. Murata, K. Sasaki, T. Kishimoto, S. Niwa, H. Hayashi, Y. Takahama, K. Tanaka, Regulation of CD8+ T cell development by thymus-specific proteasomes, Science 316 (2007) 1349–1353.
[74] S. Murata, Y. Takahama, M. Kasahara, K. Tanaka, The immunoproteasome and thymoproteasome: functions, evolution and human disease, Nat. Immunol. 19 (2018) 923–931.
[75] P.G. Richardson, P. Sonneveld, M.W. Schuster, D. Irwin, E.A. Stadtmauer, T. Facon, J.L. Harousseau, D. Ben-Yehuda, S. Lonial, H. Goldschmidt, D. Reece, J. F. San-Miguel, J. Blade, M. Boccadoro, J. Cavenagh, W.S. Dalton, A.L. Boral, D. L. Esseltine, J.B. Porter, D. Schenkein, K.C. Anderson, I. Assessment of proteasome inhibition for extending remissions, bortezomib or high-dose dexamethasone for relapsed multiple myeloma, N. Engl. J. Med. 352 (2005) 2487–2498.
[76] T.A. Guerrero-Garcia, S. Gandolfi, J.P. Laubach, T. Hideshima, D. Chauhan, C. Mitsiades, K.C. Anderson, P.G. Richardson, The power of proteasome inhibition in multiple myeloma, Exp. Rev. Proteomics 15 (2018) 1033–1052.
[77] T. Hideshima, C. Mitsiades, M. Akiyama, T. Hayashi, D. Chauhan, P. Richardson, R. Schlossman, K. Podar, N.C. Munshi, N. Mitsiades, K.C. Anderson, Molecular mechanisms mediating antimyeloma activity of proteasome inhibitor PS-341, Blood 101 (2003) 1530–1534.
[78] N. Mitsiades, C.S. Mitsiades, V. Poulaki, D. Chauhan, G. Fanourakis, X. Gu, C. Bailey, M. Joseph, T.A. Libermann, S.P. Treon, N.C. Munshi, P.G. Richardson, T. Hideshima, K.C. Anderson, Molecular sequelae of proteasome inhibition in human multiple myeloma cells, Proc. Natl. Acad. Sci. U. S. A. 99 (2002) 14374–14379.
[79] V. Cheriyath, B.S. Jacobs, M.A. Hussein, Proteasome inhibitors in the clinical setting: benefits and strategies to overcome multiple myeloma resistance to proteasome inhibitors, Drugs R D 8 (2007) 1–12.
[80] N.E. Franke, D. Niewerth, Y.G. Assaraf, J. van Meerloo, K. Vojtekova, C.H. van Zantwijk, S. Zweegman, E.T. Chan, C.J. Kirk, D.P. Geerke, A.D. Schimmer, G. J. Kaspers, G. Jansen, J. Cloos, Impaired bortezomib binding to mutant beta5 subunit of the proteasome is the underlying basis for bortezomib resistance in leukemia cells, Leukemia 26 (2012) 757–768.
[81] J. Schrader, F. Henneberg, R.A. Mata, K. Tittmann, T.R. Schneider, H. Stark, G. Bourenkov, A. Chari, The inhibition mechanism of human 20S proteasomes enables next-generation inhibitor design, Science 353 (2016) 594–598.
[82] E.M. Huber, W. Heinemeyer, M. Groll, Bortezomib-resistant mutant proteasomes: structural and biochemical evaluation with carfilzomib and ONX 0914, Structure 23 (2015) 407–417.
[83] E.M. Huber, M. Basler, R. Schwab, W. Heinemeyer, C.J. Kirk, M. Groettrup, M. Groll, Immuno- and constitutive proteasome crystal structures reveal differences in substrate and inhibitor specificity, Cell 148 (2012) 727–738.
[84] P. Sledz, W. Baumeister, Structure-Driven Developments of 26S Proteasome Inhibitors, Annu. Rev. Pharmacol. Toxicol. 56 (2016) 191–209.

[85] S. van Nocker, S. Sadis, D.M. Rubin, M. Glickman, H. Fu, O. Coux, I. Wefes, D. Finley, R.D. Vierstra, The multiubiquitin-chain-binding protein Mcb1 is a component of the 26S proteasome in Saccharomyces cerevisiae and plays a nonessential, substrate-specific role in protein turnover, Mol. Cell. Biol. 16 (1996) 6020–6028.
[86] K. Husnjak, S. Elsasser, N. Zhang, X. Chen, L. Randles, Y. Shi, K. Hofmann, K. J. Walters, D. Finley, I. Dikic, Proteasome subunit Rpn13 is a novel ubiquitin receptor, Nature 453 (2008) 481–488.
[87] Y. Shi, X. Chen, S. Elsasser, B.B. Stocks, G. Tian, B.H. Lee, Y. Shi, N. Zhang, S.A. de Poot, F. Tuebing, S. Sun, J. Vannoy, S.G. Tarasov, J.R. Engen, D. Finley, K. J. Walters, Rpn1 provides adjacent receptor sites for substrate binding and deubiquitination by the proteasome, Science (2016) 351.
[88] J. He, K. Kulkarni, P.C. da Fonseca, D. Krutauz, M.H. Glickman, D. Barford, E. P. Morris, The structure of the 26S proteasome subunit Rpn2 reveals its PC repeat domain as a closed toroid of two concentric alpha-helical rings, Structure 20 (2012) 513–521.
[89] A. Aufderheide, F. Beck, F. Stengel, M. Hartwig, A. Schweitzer, G. Pfeifer, A. L. Goldberg, E. Sakata, W. Baumeister, F. Forster, Structural characterization of the interaction of Ubp6 with the 26S proteasome, Proc. Natl. Acad. Sci. U. S. A. 112 (2015) 8626–8631.
[90] Y. Zhu, W.L. Wang, D. Yu, Q. Ouyang, Y. Lu, Y. Mao, Structural mechanism for nucleotide-driven remodeling of the AAA-ATPase unfoldase in the activated human 26S proteasome, Nat. Commun. 9 (2018) 1360.
[91] X. Wang, P. Cimermancic, C. Yu, A. Schweitzer, N. Chopra, J.L. Engel, C. Greenberg, A.S. Huszagh, F. Beck, E. Sakata, Y. Yang, E.J. Novitsky, A. Leitner, P. Nanni, A. Kahraman, X. Guo, J.E. Dixon, S.D. Rychnovsky, R. Aebersold, W. Baumeister, A. Sali, L. Huang, Molecular details underlying dynamic structures and regulation of the human 26S proteasome, Mol. Cell. Proteomics 16 (2017) 840–854.
[92] J. Querol-Audi, C. Sun, J.M. Vogan, M.D. Smith, Y. Gu, J.H. Cate, E. Nogales, Architecture of human translation initiation factor 3, Structure 21 (2013) 920–928.
[93] A. Des Georges, V. Dhote, L. Kuhn, C.U. Hellen, T.V. Pestova, J. Frank, Y. Hashem, Structure of mammalian eIF3 in the context of the 43S preinitiation complex, Nature 525 (2015) 491–495.
[94] R.I. Enchev, A. Schreiber, F. Beuron, E.P. Morris, Structural insights into the COP9 signalosome and its common architecture with the 26S proteasome lid and eIF3, Structure 18 (2010) 518–527.
[95] E. Estrin, J.R. Lopez-Blanco, P. Chacon, A. Martin, Formation of an intricate helical bundle dictates the assembly of the 26S proteasome lid, Structure 21 (2013) 1624–1635.
[96] E.J. Worden, C. Padovani, A. Martin, Structure of the Rpn11-Rpn8 dimer reveals mechanisms of substrate deubiquitination during proteasomal degradation, Nat. Struct. Mol. Biol. 21 (2014) 220–227.
[97] G.R. Pathare, I. Nagy, P. Sledz, D.J. Anderson, H.J. Zhou, E. Pardon, J. Steyaert, F. Forster, A. Bracher, W. Baumeister, Crystal structure of the proteasomal deubiquitylation module Rpn8-Rpn11, Proc. Natl. Acad. Sci. U. S. A. 111 (2014) 2984–2989.
[98] R. Verma, L. Aravind, R. Oania, W.H. McDonald, J.R. Yates 3rd, E.V. Koonin, R. J. Deshaies, Role of Rpn11 metalloprotease in deubiquitination and degradation by the 26S proteasome, Science 298 (2002) 611–615.
[99] T. Yao, R.E. Cohen, A cryptic protease couples deubiquitination and degradation by the proteasome, Nature 419 (2002) 403–407.
[100] E.J. Worden, K.C. Dong, A. Martin, An AAA Motor-Driven Mechanical Switch in Rpn11 Controls Deubiquitination at the 26S Proteasome, Mol. Cell 67 (2017) 799–811, e798.
[101] R.J. Tomko Jr., M. Funakoshi, K. Schneider, J. Wang, M. Hochstrasser, Heterohexameric ring arrangement of the eukaryotic proteasomal ATPases: implications for proteasome structure and assembly, Mol. Cell 38 (2010) 393–403.
[102] Y.A. Lam, T.G. Lawson, M. Velayutham, J.L. Zweier, C.M. Pickart, A proteasomal ATPase subunit recognizes the polyubiquitin degradation signal, Nature 416 (2002) 763–767.
[103] M.G. Rossmann, D. Moras, K.W. Olsen, Chemical and biological evolution of nucleotide-binding protein, Nature 250 (1974) 194–199.
[104] P. Wendler, S. Ciniawsky, M. Kock, S. Kube, Structure and function of the AAA+ nucleotide binding pocket, Biochim. Biophys. Acta 1823 (2012) 2–14.
[105] C. Puchades, C.R. Sandate, G.C. Lander, The molecular principles governing the activity and functional diversity of AAA+ proteins, Nat. Rev. Mol. Cell Biol. 21 (2020) 43–58.
[106] K. Karata, T. Inagawa, A.J. Wilkinson, T. Tatsuta, T. Ogura, Dissecting the role of a conserved motif (the second region of homology) in the AAA family of ATPases. Site-directed mutagenesis of the ATP-dependent protease FtsH, J. Biol. Chem. 274 (1999) 26225–26232.
[107] J.E. Walker, M. Saraste, M.J. Runswick, N.J. Gay, Distantly related sequences in the alpha- and beta-subunits of ATP synthase, myosin, kinases and other ATP-requiring enzymes and a common nucleotide binding fold, EMBO J. 1 (1982) 945–951.
[108] A.N. Kravats, S. Tonddast-Navaei, R.J. Bucher, G. Stan, Asymmetric processing of a substrate protein in sequential allosteric cycles of AAA+ nanomachines, J. Chem. Phys. 139 (2013) 121921.
[109] A. Martin, T.A. Baker, R.T. Sauer, Pore loops of the AAA+ ClpX machine grip substrates to drive translocation and unfolding, Nat. Struct. Mol. Biol. 15 (2008) 1147–1151.
[110] R. Beckwith, E. Estrin, E.J. Worden, A. Martin, Reconstitution of the 26S proteasome reveals functional asymmetries in its AAA+ unfoldase, Nat. Struct. Mol. Biol. 20 (2013) 1164–1172.
[111] J.B. Jastrab, K.H. Darwin, Bacterial Proteasomes, Annu. Rev. Microbiol. 69 (2015) 109–127.
[112] P. Majumder, W. Baumeister, Proteasomes: unfoldase-assisted protein degradation machines, Biol. Chem. 401 (2019) 183–199.
[113] Z. Merai, N. Chumak, M. Garcia-Aguilar, T.F. Hsieh, T. Nishimura, V.K. Schoft, J. Bindics, L. Slusarz, S. Arnoux, S. Opravil, K. Mechtler, D. Zilberman, R. L. Fischer, H. Tamaru, The AAA-ATPase molecular chaperone Cdc48/p97 disassembles sumoylated centromeres, decondenses heterochromatin, and activates ribosomal RNA genes, Proc. Natl. Acad. Sci. U. S. A. 111 (2014) 16166–16171.
[114] Z.A. Ripstein, R. Huang, R. Augustyniak, L.E. Kay, J.L. Rubinstein, Structure of a AAA+ unfoldase in the process of unfolding substrate, Elife (2017) 6.
[115] T. Wang, H. Li, G. Lin, C. Tang, D. Li, C. Nathan, K.H. Darwin, H. Li, Structural insights on the Mycobacterium tuberculosis proteasomal ATPase Mpa, Structure 17 (2009) 1377–1385.
[116] S. Djuranovic, M.D. Hartmann, M. Habeck, A. Ursinus, P. Zwickl, J. Martin, A. N. Lupas, K. Zeth, Structure and activity of the N-terminal substrate recognition domains in proteasomal ATPases, Mol. Cell 34 (2009) 580–590.
[117] D. Haselbach, J. Schrader, F. Lambrecht, F. Henneberg, A. Chari, H. Stark, Long-range allosteric regulation of the human 26S proteasome by 20S proteasome-targeting cancer drugs, Nat. Commun. 8 (2017) 15578.
[118] Z. Ding, Z. Fu, C. Xu, Y. Wang, Y. Wang, J. Li, L. Kong, J. Chen, N. Li, R. Zhang, Y. Cong, High-resolution cryo-EM structure of the proteasome in complex with ADP-AlFx, Cell Res. 27 (2017) 373–385.
[119] B. Luan, X. Huang, J. Wu, Z. Mei, Y. Wang, X. Xue, C. Yan, J. Wang, D.J. Finley, Y. Shi, F. Wang, Structure of an endogenous yeast 26S proteasome reveals two major conformational states, Proc. Natl. Acad. Sci. U. S. A. 113 (2016) 2642–2647.
[120] X. Huang, B. Luan, J. Wu, Y. Shi, An atomic structure of the human 26S proteasome, Nat. Struct. Mol. Biol. 23 (2016) 778–785.
[121] X. Chen, Z. Dorris, D. Shi, R.K. Huang, H. Khant, T. Fox, N. de Val, D. Williams, P. Zhang, K.J. Walters, Cryo-EM reveals unanchored M1-ubiquitin chain binding at hRpn11 of the 26S proteasome, Structure 28 (2020) 1206–1217, e1204.
[122] M.R. Eisele, R.G. Reed, T. Rudack, A. Schweitzer, F. Beck, I. Nagy, G. Pfeifer, J. M. Plitzko, W. Baumeister, R.J. Tomko Jr., E. Sakata, Expanded coverage of the 26S Proteasome conformational landscape reveals mechanisms of peptidase gating, Cell Rep. 24 (2018) 1301–1315, e1305.
[123] P. Sledz, P. Unverdorben, F. Beck, G. Pfeifer, A. Schweitzer, F. Forster, W. Baumeister, Structure of the 26S proteasome with ATP-gammaS bound provides insights into the mechanism of nucleotide-dependent substrate translocation, Proc. Natl. Acad. Sci. U. S. A. 110 (2013) 7264–7269.
[124] E.R. Greene, K.C. Dong, A. Martin, Understanding the 26S proteasome molecular machine from a structural and conformational dynamics perspective, Curr. Opin. Struct. Biol. 61 (2020) 33–41.
[125] D. Finley, M.A. Prado, The proteasome and its network: engineering for adaptability, Cold Spring Harb. Perspect. Biol. (2020) 12.
[126] D. Finley, X. Chen, K.J. Walters, Gates, channels, and switches: Elements of the proteasome machine, Trends Biochem. Sci. 41 (2016) 77–93.
[127] C.R. Sandate, A. Szyk, E.A. Zehr, G.C. Lander, A. Roll-Mecak, An allosteric network in spastin couples multiple activities required for microtubule severing, Nat. Struct. Mol. Biol. 26 (2019) 671–678.
[128] C.M. Ho, J.R. Beck, M. Lai, Y. Cui, D.E. Goldberg, P.F. Egea, Z.H. Zhou, Malaria parasite translocon structure and mechanism of effector export, Nature 561 (2018) 70–75.
[129] E.C. Twomey, Z. Ji, T.E. Wales, N.O. Bodnar, S.B. Ficarro, J.A. Marto, J.R. Engen, T.A. Rapoport, Substrate processing by the Cdc48 ATPase complex is initiated by ubiquitin unfolding, Science (2019) 365.
[130] I. Cooney, H. Han, M.G. Stewart, R.H. Carson, D.T. Hansen, J.H. Iwasa, J.C. Price, C.P. Hill, P.S. Shen, Structure of the Cdc48 segregase in the act of unfolding an authentic substrate, Science 365 (2019) 502–505.
[131] A.L. Yokom, S.N. Gates, M.E. Jackrel, K.L. Mack, M. Su, J. Shorter, D. R. Southworth, Spiral architecture of the Hsp104 disaggregase reveals the basis for polypeptide translocation, Nat. Struct. Mol. Biol. 23 (2016) 830–837.
[132] S.N. Gates, A.L. Yokom, J. Lin, M.E. Jackrel, A.N. Rizo, N.M. Kendsersky, C. E. Buell, E.A. Sweeny, K.L. Mack, E. Chuang, M.P. Torrente, M. Su, J. Shorter, D. R. Southworth, Ratchet-like polypeptide translocation mechanism of the AAA+ disaggregase Hsp104, Science 357 (2017) 273–279.
[133] C. Puchades, A.J. Rampello, M. Shin, C.J. Giuliano, R.L. Wiseman, S.E. Glynn, G. C. Lander, Structure of the mitochondrial inner membrane AAA+ protease YME1 gives insight into substrate processing, Science 358 (2017).
[134] P. Majumder, T. Rudack, F. Beck, R. Danev, G. Pfeifer, I. Nagy, W. Baumeister, Cryo-EM structures of the archaeal PAN-proteasome reveal an around-the-ring ATPase cycle, Proc. Natl. Acad. Sci. U. S. A. 116 (2019) 534–539.
[135] S. Augustin, F. Gerdes, S. Lee, F.T. Tsai, T. Langer, T. Tatsuta, An intersubunit signaling network coordinates ATP hydrolysis by m-AAA proteases, Mol. Cell 35 (2009) 574–585.
[136] J.A.M. Bard, C. Bashore, K.C. Dong, A. Martin, The 26S Proteasome Utilizes a Kinetic Gateway to Prioritize Substrate Degradation, Cell 177 (2019) 286–298, e215.
[137] B.D. Engel, M. Schaffer, L. Kuhn Cuellar, E. Villa, J.M. Plitzko, W. Baumeister, Native architecture of the Chlamydomonas chloroplast revealed by in situ cryo-electron tomography, Elife (2015) 4.

[138] B.D. Engel, M. Schaffer, S. Albert, S. Asano, J.M. Plitzko, W. Baumeister, In situ structural analysis of Golgi intracisternal protein arrays, Proc. Natl. Acad. Sci. U. S. A. 112 (2015) 11264–11269.
[139] S. Mosalaganti, J. Kosinski, S. Albert, M. Schaffer, D. Strenkert, P.A. Salome, S. S. Merchant, J.M. Plitzko, W. Baumeister, B.D. Engel, M. Beck, In situ architecture of the algal nuclear pore complex, Nat. Commun. 9 (2018) 2361.
[140] Q. Guo, C. Lehmer, A. Martinez-Sanchez, T. Rudack, F. Beck, H. Hartmann, M. Perez-Berlanga, F. Frottin, M.S. Hipp, F.U. Hartl, D. Edbauer, W. Baumeister, R. Fernandez-Busnadiego, In situ structure of neuronal C9orf72 Poly-GA aggregates Reveals proteasome recruitment, Cell 172 (2018) 696–705, e612.
[141] D.A. Kraut, E. Israeli, E.K. Schrader, A. Patil, K. Nakai, D. Nanavati, T. Inobe, A. Matouschek, Sequence- and species-dependence of proteasomal processivity, ACS Chem. Biol. 7 (2012) 1444–1453.
[142] J. Levitskaya, A. Sharipo, A. Leonchiks, A. Ciechanover, M.G. Masucci, Inhibition of ubiquitin/proteasome-dependent protein degradation by the Gly-Ala repeat domain of the Epstein-Barr virus nuclear antigen 1, Proc. Natl. Acad. Sci. U. S. A. 94 (1997) 12616–12621.
[143] S. Yasuda, H. Tsuchiya, A. Kaiho, Q. Guo, K. Ikeuchi, A. Endo, N. Arai, F. Ohtake, S. Murata, T. Inada, W. Baumeister, R. Fernandez-Busnadiego, K. Tanaka, Y. Saeki, Stress- and ubiquitylation-dependent phase separation of the proteasome, Nature 578 (2020) 296–300.
[144] F. Forster, P. Unverdorben, P. Sledz, W. Baumeister, Unveiling the long-held secrets of the 26S proteasome, Structure 21 (2013) 1551–1562.
[145] S Albert, M Schaffer, F Beck, S Mosalaganti, S Asano, H Thomas, M.J Plitzko, M Beck, W Baumeister, D.B Engel, et al., Proteasomes tether to two distinct sites at the nuclear pore complex, Proc. Natl. Acad. Sci. U. S. A. 114 (52) (2017) 13726–13731.
[146] S Albert, W Wietrzynski, C Lee, M Schaffer, F Beck, M.J Schuller, A.P Salome, M. J Plitzko, W Baumeister, D.B Engel, Direct visualization of degradation microcompartments at the ER membrane, Proc. Natl. Acad. Sci. U. S. A. 14 (117) (2020) 1069–1080.